INITIAL RESULTS FROM THE TOKAPOLE II POLOIDAL DIVERTOR EXPERIMENT

A.P. Biddle, R.N. Dexter, R.J. Groebner, D.J. Holly,
B. Lipschultz, M.W. Phillips, S.C. Prager, and J.C. Sprott

PLP 788

February 1979

Plasma Studies

University of Wisconsin

INITIAL RESULTS FROM THE TOKAPOLE II POLOIDAL DIVERTOR EXPERIMENT

A.P. Biddle, R.N. Dexter, R.J. Groebner, D.J. Holly,
B. Lipschultz, M.W. Phillips, S.C. Prager, and J.C. Sprott

COO-2387-103

February 1979

INITIAL RESULTS FROM THE TOKAPOLE II POLOIDAL DIVERTOR EXPERIMENT

A.P. Biddle, R.N. Dexter, R.J. Groebner, D.J. Holly,
B. Lipschultz, M.W. Phillips, S.C. Prager, and J.C. Sprott

University of Wisconsin, Madison, Wisconsin, USA

ABSTRACT

The latest in a series of internal ring devices, called Tokapole II, has recently begun operation at the University of Wisconsin. Its purpose is to permit the study of the production and confinement of hot, dense plasmas in either a toroidal octupole (with or without toroidal field) or a tokamak with a four-node poloidal divertor. The characteristics of the device and the results of its initial operation are described here. Quantitative measurements of impurity concentration and radiated power have been made. Poloidal divertor equilibria of square and dee shapes have been produced, and an axisymmetric instability has been observed with the inverse dee. Electron cyclotron resonance heating is used to initiate the breakdown near the axis and to control the initial influx of impurities. A 2 MW rf source at the second harmonic of the ion cyclotron frequency is available and has been used to double the ion temperature when operated at low power with an unoptimized antenna. Initial results of operation as a pure octupole with poloidal ohmic heating suggest a tokamak-like scaling of density ($n \propto B_p$) and confinement time ($\tau \propto n$).

I. INTRODUCTION

Internal ring devices (multipoles, spherators, levitrons, and surmacs) have a long and impressive history of contributions to the understanding of magnetically-confined, toroidal plasmas. Most of the experiments have used relatively cold (few eV), low density (10^{9}-10^{12} cm^{-3}) plasmas, not out of necessity, however, but rather as an experimental convenience. With the progress in heating and impurity control in tokamaks and the renewed interest in internal ring devices as advanced fuel reactors and as poloidal divertors for tokamaks, it seemed timely to construct a new internal ring device specifically to produce and confine hot (few hundred eV), dense (10^{13} cm^{-3}) plasmas. The device, called Tokapole II, is basically an octupole with a relatively strong (up to 10 kG) toroidal field. By controlling the shape and timing of the octupole and toroidal fields, the device can be operated as an octupole (with or without toroidal field), or as a tokamak with a four-node poloidal divertor. Poloidal divertor configurations with square or dee-shaped cross sections can be produced by adjusting the positions of the internal rings. Plasma in the divertor region can be retained or suppressed by use of a retractable scrape-off plate. The octupole case can be studied with or without ohmic heating. The versatility of the device allows a direct comparison of a wide variety of magnetic configurations in a device of the same size, field strength, wall cleanliness, etc. This paper will describe the device and initial measurements of the plasma characteristics, with particular emphasis on its operation as a tokamak with a poloidal divertor. Studies of electron cyclotron resonance breakdown and high power rf heating at the second harmonic of the ion cyclotron frequency will be discussed. Initial results of density and energy confinement time scaling for the pure octupole with poloidal ohmic heating will also be given.

II. DEVICE DESCRIPTION

The Tokapole II device consists of a 50 cm major radius, 44 × 44 cm square cross section, 3 cm thick, aluminum, toroidal vacuum vessel which is linked by an 0.15 volt-sec iron transformer core as shown in Fig. 1. The vacuum chamber walls have a field soak-in time of about 15 msec, thus insuring a high degree of magnetic symmetry for the field pulse lengths used. This magnetic symmetry was preserved by machining the vacuum tank to a high precision (0.5 mm) and paying careful attention to the placement of the toroidal and poloidal field primary windings in the vicinity of the toroidal and poloidal voltage gaps. A total of 42 ports was provided to facilitate diagnostic access, and the ports were arranged wherever possible in pairs on the top and bottom so as to preserve symmetry about the horizontal midplane. The perturbations caused by the larger (19 cm diameter) pump ports are minimized by the use of 55% transparent copper plugs which have the same average resistivity as the aluminum walls.

The octupole field is produced by four, 5 cm diameter, solid copper hoops which encircle the iron core and can carry a total peak current of up to 700 kA. The hoops were machined to a high tolerance (0.13 mm) and polished. The hoops are positioned carefully near the corners of the vacuum vessel so that the three field nulls coalesce into a single octupole null near the minor axis as shown in Fig. 2. Experiments on an earlier device,[1] Tokapole I, which was operated as an octupole (four hoops), a quadrupole (two hoops), and a tokamak (no hoops) indicated the difficulty of driving toroidal plasma currents in a low order field null, as shown in Fig. 3. Each hoop is supported by three beryllium-copper rods which are threaded to allow a vertical adjustment of ± 5 mm of each hoop position. The total support area of 133 cm^2 limits the confinement time of 100 eV ions in the divertor region to about 1.5 msec. A retractable divertor scrape-off plate with a total area of 240 cm^2 (each side) is also available. The hoops are

electrically insulated from the vacuum chamber and can be biased up to 10 kV. A 90 kJ capacitor bank, which can produce up to 125 volts across the poloidal gap, is used to excite the poloidal field.

The toroidal field winding consists of 96 turns of AWG 4/0 welding cable and is secured to the vacuum chamber by 24 sets of aluminum channels as shown in Fig. 1. The mechanical strength is sufficient to permit toroidal fields of up to 10 kG on axis, but the existing 126 kJ capacitor bank limits the field to 5 kG. A peak field on axis of ~ 3.7 kG was used for most of the experiments described here. Both the toroidal and poloidal fields can be crowbarred with a decay time of ~ 20 msec.

A base vacuum of ~ 3×10^{-8} torr is achieved with a 1500 ℓ/sec turbomolecular pump and a 1200 ℓ/sec 10° K cryopump. All vacuum seals are viton, but care is taken to insure that the only insulators exposed to the plasma are ceramic. Provisions were incorporated for baking the entire machine to 150° C, but so far the bake has been limited to 50° C. A residual gas analyzer typically shows water to be the dominant impurity. Discharge cleaning is accomplished by pulsing the toroidal field to about 1 kG every two seconds and ringing the poloidal gap with a decaying sine wave of about 50 volts and a frequency of about 3 kHz.

A more detailed description of the device is available elsewhere.[2] Table I summarizes the main characteristics of the device.

TABLE 1

Major radius: 50 cm

Minor cross section: 44 × 44 cm square

Toroid walls: aluminum, 3 cm thick with poloidal and toroidal insulated gaps

Vacuum volume: 600 liters

Vacuum surface area: 6 square meters

Number of internal rings: 4 (copper, 5 cm diameter, supported at 3 points)

Ports: 2 - 19 cm diam, 5 - 11.5 cm diam, 22 - 4 cm diam, 13 - 0.6 cm diam

B_T on axis: 5 kG (extendable to 10 kG by the acquisition of additional capacitors)

L/R time of B_T: 20 msec

Available OH voltage: 125 volts

Poloidal flux: 0.15 webers

Available energy (poloidal + toroidal fields): 216 kJ (72 - 240 μF, 5 kV capacitors)

Base vacuum: 3×10^{-8} torr

Pumping system: 1500 ℓ/sec turbomolecular pump

1200 ℓ/sec, 10° K cryopump

Preionization: 5 kW, 2.45 GHz; 10 kW, 8.8 GHz; 10 kW, 16.0 GHz

III. DIAGNOSTICS

Since the internal rings and plasma both link the ohmic heating transformer, the measurements of the plasma loop voltage and current are not straightforward. A special magnetic probe is used to determine the loop voltage. The plasma current is measured with a large Rogowskii loop which encloses the region between the rings. Also, an appropriate circuit model, including the plasma (assumed localized near the minor axis) and the rings, allows us to infer the plasma current by measurement of the poloidal gap voltage and the ohmic heating primary current. Electron density is measured with Langmuir probes and a 40 GHz phase-shift microwave interferometer. The interferometer signal is cut off at the maximum density.

Spectroscopic diagnostics include a 1/2-m Jarrell-Ash monochromator, a 1/2-m Seya-Namioka vacuum ultraviolet (VUV) spectrometer, a 1-m Seya VUV monochromator, and a variety of filters and detectors. The 1/2-m Seya is equipped with a phosphor-coated microchannel plate so that we can obtain a panoramic view of the spectral region from 400 - 1250 Å in one shot. This output can be photographed or displayed on a TV screen by a gated storage vidicon. The 1-m Seya has been absolutely calibrated and is used to measure impurity line-radiated power. An absolute calibration for the 1/2-m Seya has been inferred from power measurements with the 1-m instrument.

Ion temperature (T_i) is determined from the Doppler broadening of visible lines of impurity ions and from the He II λ4686 Å line. Electron temperature (T_e) is determined with the aid of a computer code which models the observed ionization state sequence of OIII through OVI. This technique has been described elsewhere.[3]

IV. DISCHARGE CHARACTERISTICS

Figure 4a indicates the timing of the fields and preionization for a typical discharge. A fast piezoelectric valve is used to fill the machine with about 3×10^{-4} torr of hydrogen. About 12.7 msec later, the toroidal field is triggered and is crowbarred when it reaches its peak field strength. Shortly before peak field, a 1 msec pulse of 10 kW, 8.8 GHz microwaves is used as preionization. The ohmic heating voltage, which is sinusoidal in time with a quarter-period of 2.8 msec, is triggered during the preionization pulse.

Figure 4b displays a plasma current (I_p) trace. This yields a peak current of about 40 kA, while the Rogowskii loop gives a peak I_p of about 20 kA indicating that a considerable amount of current flows in the common flux region around the rings. The line-averaged T_e, as determined by the method described above, is also shown in Fig. 4b. T_e is low during the formation of the central current channel and rises to 100 eV or more once the current channel has been formed. T_i is about 15 eV and is constant during the central part of the discharge. The peak, spatially-averaged, electron density is about 1×10^{13} cm^{-3}.

The ohmic input power is high throughout the discharge and reaches a peak of about 400 kW. With the best data available, we estimate that the total energy confinement time (τ_E) is about 200 μsec.

V. IMPURITY MEASUREMENTS

In an effort to understand the energy loss mechanisms, we have made qualitative and quantitative impurity line radiation measurements. The major impurities are oxygen, carbon, nitrogen (associated with vacuum leaks), copper, and aluminum. Typical impurity concentrations are shown in Table II. The densities of the metal impurities have not been determined. Z_{eff} is estimated to be ~ 2.5-3.5. The total line radiated power in the 500-1250 Å region is about 70 kW, while radiation in the soft x-ray region has been determined to

TABLE II

Impurity	Density
Oxygen:	3×10^{11} cm^{-3}
Nitrogen:	2×10^{11} cm^{-3}
Carbon:	5×10^{10} cm^{-3}

be only a small fraction of that in the VUV. These measurements indicate, that within our margins of error, line radiation is not the dominant energy loss mechanism.

More likely the energy losses are related to the low value of the safety factor, q, in our discharges. On axis, q is of order unity. It has been shown on ORMAK,[4] that $\tau_E \sim \sqrt{q(a)}$, where q(a) is the safety factor at the limiter, for q(a) less than about 6. It remains for us to study the variation of τ_E with safety factor.

VI. EQUILIBRIUM AND STABILITY OF A POLOIDAL DIVERTOR CONFIGURATION

Divertor configurations are becoming more important as solutions to the impurity problems now besetting tokamaks. One such configuration is the poloidal divertor where poloidal flux is diverted axisymmetrically and plasma outside the separatrix is scraped off. The poloidal divertor configuration which is by nature noncircular is also advantageous with respect to q-limited and β-limited MHD modes. However the noncircular nature of this configuration makes it unstable to axisymmetric displacements (circular plasmas are neutrally stable). The importance of these axisymmetric modes is apparent and has given rise to a fairly large amount of linear theory using the energy principle--mostly for idealized displacements of ideal analytic equilibria and for numerically calculated equilibria using Princeton's stability code (PEST).[4,5,6] Recently the nonlinear evolution of the instability has been followed by Jardin[7] by the numerical integration of the two-dimensional, axisymmetric, time-dependent, ideal MHD equation in toroidal geometry. Axisymmetric displacements of dee[8] and elliptical[9,10] plasmas have been deduced in a few previous experiments from magnetic probes external to the plasma. Plasma shapes and positions have been inferred from equilibrium computer codes using external experimental signals as input.

We have made the first direct experimental observation of the stability to axisymmetric modes of square and inverse dee shaped equilibria in a 4-null poloidal divertor configuration.[11] Equilibrium is verified by mapping the flux

plot as a function of time and its stability is determined by studying the evolution of these flux plots. We have found that inverse dee and square shaped equilibria exist and that inverse dee shaped equilibria are more unstable than the square equilibria. Growth times for the inverse dee are ~ 1000 poloidal Alfvén times implying that passive stabilization due to the rings and walls has occurred.

As part of the program to study the equilibrium and stability of poloidal divertor configurations, an axisymmetric magnetohydrodynamic equilibrium code was written to handle internal ring devices with current carrying plasmas such as the Tokapole II. This code solves the Grad Shafranov equation for the poloidal flux, ψ, given pressure and poloidal current as functions of ψ and subject to the proper boundary conditions outside the plasma. The plasma is assumed to be confined in the central region of the torus in a divertor configuration where the boundary of the plasma is one of the separatrices. Since the plasma/vacuum interface must be solved as part of the problem, this is a free boundary type of problem. Since these problems are nonlinear, it is necessary to use iteration techniques to find the solution. The current in the rings and the plasma is induced inductively so the proper representation of the internal rings is to take their surfaces to be Dirichlet boundaries. Hence the currents in the rings will be coupled to the plasma providing some degree of wall stabilization.

A sample calculation for one of the standard ring configurations and for typical Tokapole II parameters is shown in Fig. 5. The general tendency of the plasma is to lean against the outside rings with the resulting image currents (in the rings and wall) providing a vertical field to keep the plasma centrally located.

Because internal probes may be used as a diagnostic, Tokapole II provides the opportunity to verify first hand the shape and subsequent development of its

various equilibria configurations. Figure 6 shows one such experimentally determined flux plot for roughly the same parameters and ring placement as the sample computer calculation. The values of poloidal flux in this plot were found by integrating measurements of the poloidal magnetic field. As can be seen, the agreement is fairly good.

VII. ELECTRON CYCLOTRON RESONANCE BREAKDOWN

Ten kW of 8.8 GHz ECRH is applied before the ohmic heating begins, as shown in Fig. 4. Since at this time the magnetic field is purely toroidal and is roughly constant in time, the ECRH resonance zone is a vertical cylinder. By varying the strength of the toroidal field, the resonance zone can be positioned at different radii. By thus starting the discharge with ECRH, impurity radiation can be reduced by up to about 50% compared to an ohmic discharge without ECRH preionization.

Langmuir probe traces (Fig. 7) taken with no poloidal (ohmic heating) field show that ECRH results in a plasma profile which peaks at the resonance zone as expected. This is also verified by visible light photographs of the ECRH plasma. However, when some ohmic heating is added, Langmuir probe measurements show little difference with and without the preionization (Fig. 8). Photographs of the plasma also show no change due to the preionization once the ohmic heating power has been applied.

However, impurity radiation does show a marked decrease for the first few milliseconds of the discharge when the ECRH preionization is used. The effect of the ECRH preionization on impurity radiation is a function of the position of the ECRH resonance location. Figure 9 shows the percent decrease in VUV radiation when ECRH preionization was used, relative to the case with no preionization, as the resonance zone was swept across the machine by varying the toroidal field strength. The effect of the ECRH is to decrease the impurity radiation as much

as 50% compared to the no-preionization case. Surprisingly, the effect is most pronounced when the resonance zone intersects the hoops.

The intensity of the Cu I radiation line is also much enhanced when the preionization resonance zone intersects the copper hoops. This effect persists for the duration of the discharge. Gross plasma parameters, such as the plasma current, are affected much less by the preionization (usually 10% or less). This may be in part due to the hoops producing a central current channel with a stable equilibrium, accomplishing the same result as the ECRH preionization. Thus the effect of ECRH preionization might be more dramatic in a tokamak without a poloidal divertor.

VIII. ION CYCLOTRON RESONANCE HEATING

Tokapole II is providing a unique opportunity for the study of several phases of high power ICRF heating in a plasma which has a rectangular cross section and nearly uniform density within the current channel. The 29 cm plasma cross section is surrounded by a 7.5 cm blanket of reduced density outside the magnetic limiters. As a result, toroidal eigenmodes in the vicinity of the ion cyclotron frequency are few enough to be unambiguously identifed and mapped by rf field probe measurements. The relatively large evanescent region allows detailed studies of wave coupling when the antenna is separated from the dense core of the plasma. Excellent agreement has been found between the theoretical and experimental wave modes (Figs. 10 and 11).

These studies are being done with a 2 MW self-excited rf source with a 1.2 msec square pulse length and a temporary antenna located physically outside the vacuum tank and which views the plasma through a 19 cm diameter ceramic window. As the antenna is also the inductor of the tank circuit, the oscillator frequency tends to track changes in plasma reactance thereby broadening the modes. Operation at 2 ω_{ci} in a hydrogen plasma has doubled the ion temperature

as measured by Doppler broadening of the 4686 Å line of doped helium (Fig. 12). This represents ~ 10% coupling to the ions, with the balance of the power tentatively identified with plasma edge and tank wall deposition. Impurity line radiation is seen to scale with applied power. However, no disruption of the plasma has resulted from the impurity influx. In fact, a characteristic of the Tokapole II device is that major disruptions which result in complete loss of the plasma do not occur. This may be due to the stable multipole region which surrounds the toroidal current channel.

Upgrading the launching structure to one whose separation from the plasma is continuously variable and increasing the toroidal field are expected to dramatically increase coupling efficiencies as well as allow heating in an H-D plasma with greatly reduced edge heating. The relatively low poloidal flux is expected to limit maximum ion temperatures however.

IX. PURE OCTUPOLE OPERATION

Multipoles are of considerable interest as advanced fuel reactors because a stable equilibrium can be obtained without the need for a toroidal field. Furthermore, the poloidal magnetic field has a low average value, and so the synchrotron radiation which would result at the high temperatures needed to burn the advanced fuels (several hundred keV) can be reduced to a tolerable level. However, very little is known about the scaling of energy confinement of hot, dense plasmas in a pure multipole configuration. The Tokapole II has provided an opportunity to extend the extensive measurements at low temperatures and densities into more reactor-like regimes.

In order to do this, the timing sequence of the magnetic fields is changed somewhat from that shown in Fig. 4. The discharge is initiated in a manner similar to that used for the tokamak studies, but after a hot, dense plasma is

created, the toroidal field is abruptly (~ 1 msec) reduced to zero. This abrupt decrease in toroidal field drives current poloidally and produces additional ohmic heating. Such poloidal ohmic heating may have distinct advantages over the toroidal ohmic heating used in tokamaks and stellarators. The resistivity is greatly enhanced (typically a hundredfold) by the strong magnetic mirrors. Additionally, the Krushkal-Shafranov limit presumably does not preclude arbitrarily large values of ohmic heating.

After the toroidal field reaches zero, one is left with a plasma with parameters similar to those previously described but in a pure octupole field with no ohmic heating. The subsequent decay of the plasma can then be studied. The first such experiments used a specially shaped Langmuir probe which extends across the bridge region (the narrow region between a hoop and the wall shown in Fig. 2) so as to volume-average the plasma density.

In Fig. 13 is shown the density measured as described at the end of the poloidal ohmic heating pulse as a function of the total current in the hoops (which is a measure of the poloidal field strength). An approximate linear scaling is observed ($n \propto B_p$) which resembles the scaling of density with toroidal field which is observed in tokamaks. The ion saturation current to the probe is observed to subsequently decay in an approximately exponential manner with a decay time τ which is plotted as a function of initial density in Fig. 14. Again, note the approximate linear dependence ($\tau \propto n$) at the higher densities which is characteristic of many tokamak experiments. Since the ion saturation current is proportional to $n \sqrt{T_e}$, the measured τ is a mean between the particle and energy confinement times. These results suggest that a multipole with poloidal ohmic heating enjoys the same favorable scaling as tokamaks.

X. SUMMARY AND CONCLUSIONS

The Tokapole II device is a small, low field tokamak with a four-node poloidal divertor and the additional flexibility of operating as a pure octupole. Toroidal field and ohmic heating can be used or not as desired. The general discharge characteristics agree favorably with those of similar tokamaks. Spectroscopic measurements show that impurity line radiation cannot account for more than ~ 20% of the losses. Divertor configurations of square and inverse dee shapes can be produced, and the inverse dee is observed to develop an axisymmetric instability in which the magnetic axis moves toward one of the divertor rings on a time scale of ~ 1000 poloidal Alfvén times. The square case appears to be stable. One novel feature of the experiment is the use of ECRH preionization which helps to initiate the ohmic discharge away from the walls resulting in a 50% reduction in impurity radiation. A 2MW ICRH source is available, and has been used to double the ion temperature, but with poor coupling efficiency resulting from the lack of a proper antenna. When operated as a pure octupole, the density and confinement time obey a tokamak-like scaling. Future work will include doubling the toroidal field strength and discharge length, increasing the ICRH power coupled to the plasma, studying the stability of the various poloidal divertor configurations at high beta and low q, and determining the scaling and limitations of poloidal ohmic heating.

XI. ACKNOWLEDGMENTS

We are grateful to K. Miller, T. Osborne, M. Sengstacke, D. Shepard, and D. Witherspoon for assistance in assembly of the apparatus and some diagnostic measurements. Engineering and technical support was provided by T. Lovell and R. Vallem. This work was supported by the U.S. Department of Energy.

REFERENCES

[1] R.A. DORY, D.W. KERST, D.M. MEADE, W.E. WILSON, and C.W. ERICKSON, Phys. Fluids 9, 997 (1966).

[2] J.C. SPROTT, Proceedings of the Small Toroidal Devise Users' Meeting in Monterey, Cal., May 18, 1978.

[3] Equipe TFR, Nucl. Fusion 15, 1053 (1975).

[4] L.A. BERRY, et al. in Plasma Physics and Controlled Nuclear Fusion Research (Proc. 6th Int. Conf. Berchtesgaden, 1976) 1, IAEA, 49 (1977).

[5] C. BERNARD, D. BERGER, R. GRUBER, and F. TROYON, Gulf General Atomic Report GA-A1485 (1978).

[6] J. MANICKAM, S. DALHED, J. DELUCIA, R.C. GRIMM, V.Y. HSIEH, S.C. JARDIN, J.L. JOHNSON, M. OKABAYASHIG, A.M.M. TODD, and K.E. WEIMER, Bull. Am. Phys. Soc. 23, 897 (1978).

[7] S.C. JARDIN, J.L. JOHNSON, J.M. GREENE, and R.C. GRIMM, Journal of Computational Physics 29, pp. 101-126 (1978).

[8] D. TOYAMA et al., Plasma Physics and Controlled Fusion Research 1, IAEA (1977), p. 323.

[9] G. CIMA, D.C. ROBINSON, C.L. THOMAS, A.J. WOOTON, ibid., p. 335.

[10] A.J. WOOTON, Nucl. Fusion 18 (1978), p. 1161.

[11] B. LIPSCHULTZ, et al. submitted to Phys. Rev. Letters.

FIGURE CAPTIONS

Fig. 1. The Tokapole II device.

Fig. 2. Poloidal magnetic flux plot in the absence of plasma currents.

Fig. 3. Toroidal current as a function of loop voltage for Tokapole I with four hoops (octupole), two hoops (quadrupole), and no hoops (tokamak).

Fig. 4. Time sequence of typical discharge.

Fig. 5. Numerically calculated poloidal flux plot with a plasma current.

Fig. 6. Experimentally measured poloidal flux plot in the region near the magnetic axis.

Fig. 7. Spatial profiles of ion saturation current for the ECRH preionization plasma for various resonance zone positions.

Fig. 8. Spatial profiles of ion saturation current just before and at various times after the initiation of the ohmic discharge with and without ECRH preionization.

Fig. 9. Percentage decrease in VUV radiation as a function of the ECRH resonance zone location.

Fig. 10. Dispersion relation for the fast magnetsonic wave at $\omega = \omega_{ci}$ in Tokapole II.

Fig. 11. Measured value of the spatial variation of the rf magnetic field showing the radial structure of the toroidal eigenmode.

Fig. 12. Ion temperature vs time with and without ICRH as determined by Doppler broadening of the He II 4686 Å line.

Fig. 13. Density as a function of poloidal magnetic field for the pure octupole with poloidal ohmic heating.

Fig. 14. Confinement time vs density for the pure octupole configuration.

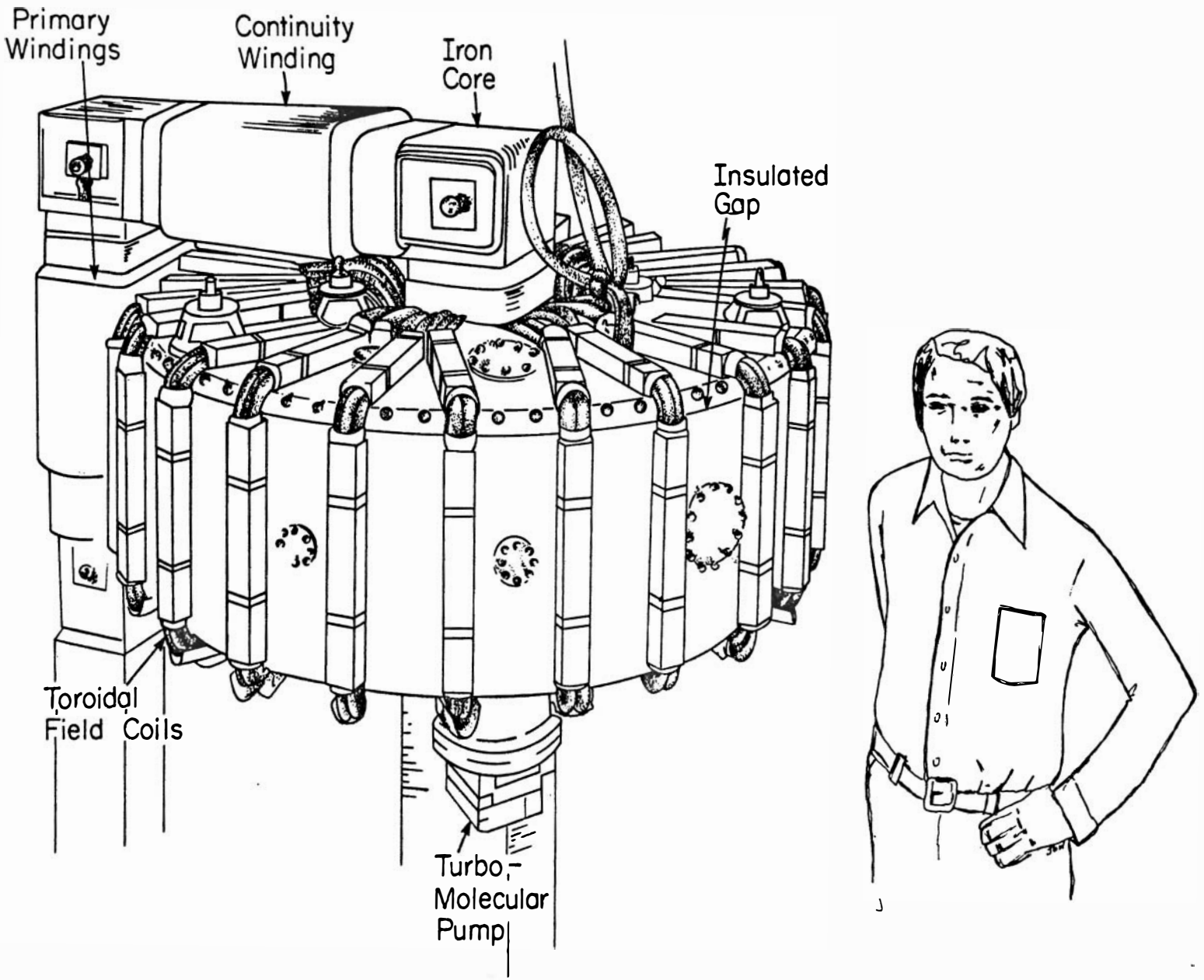
Primary Windings
Continuity Winding
Iron Core
Insulated Gap
Toroidal Field Coils
Turbo-Molecular Pump

FIGURE 1

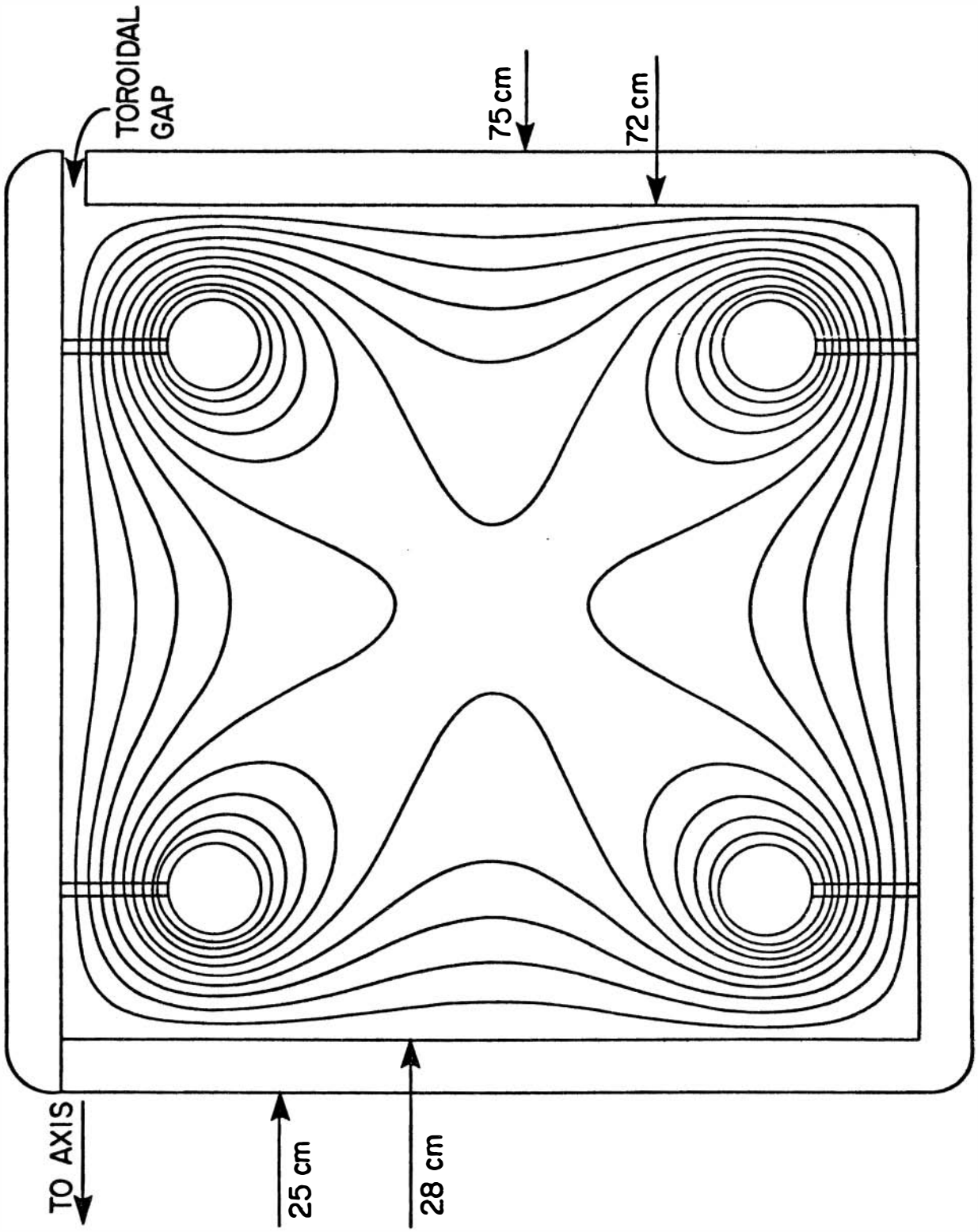

FIGURE 2

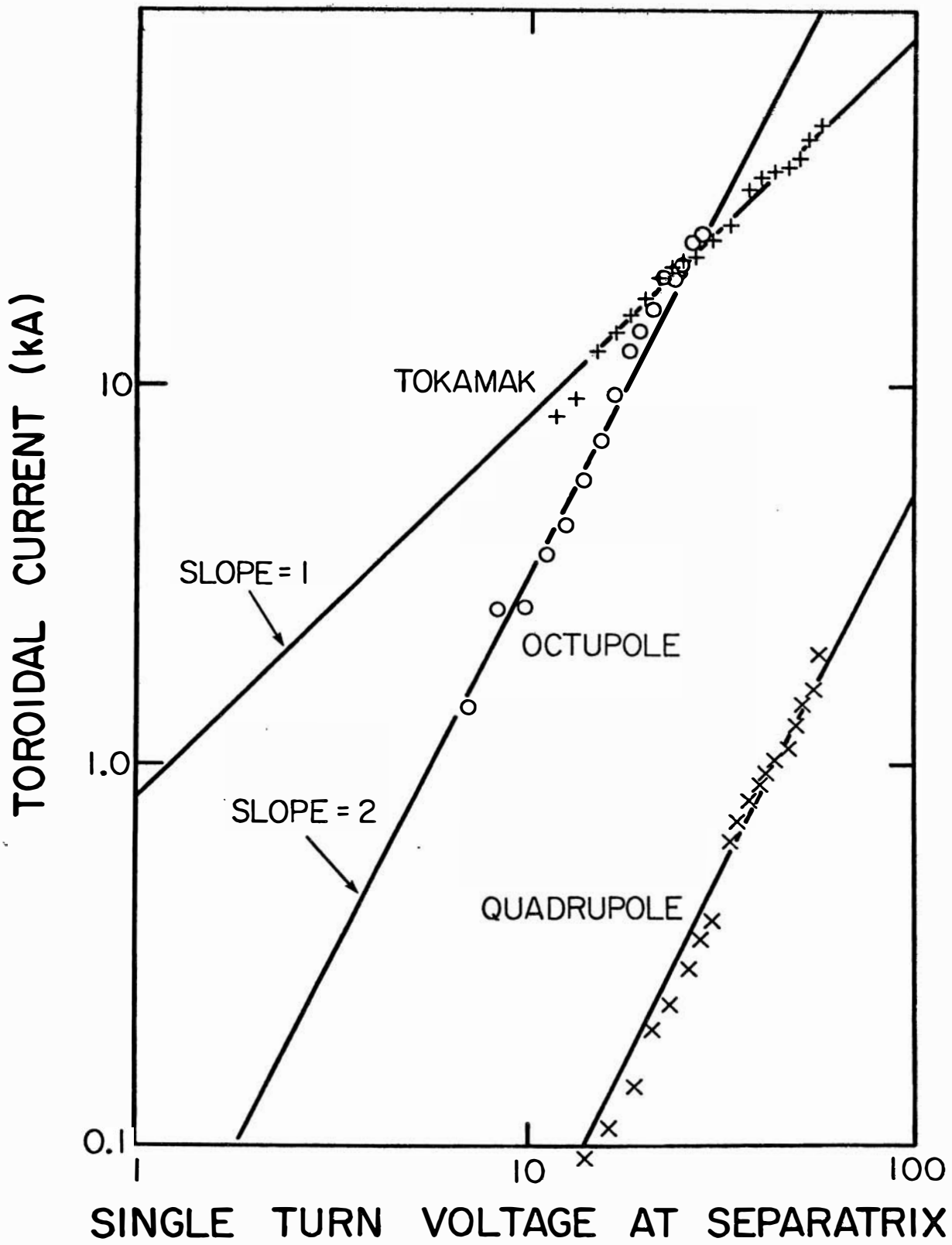
TOROIDAL CURRENT (kA)
10
1.0
0.1
TOKAMAK
SLOPE = 1
OCTUPOLE
SLOPE = 2
QUADRUPOLE
1
10
100
SINGLE TURN VOLTAGE AT SEPARATRIX

FIGURE 3

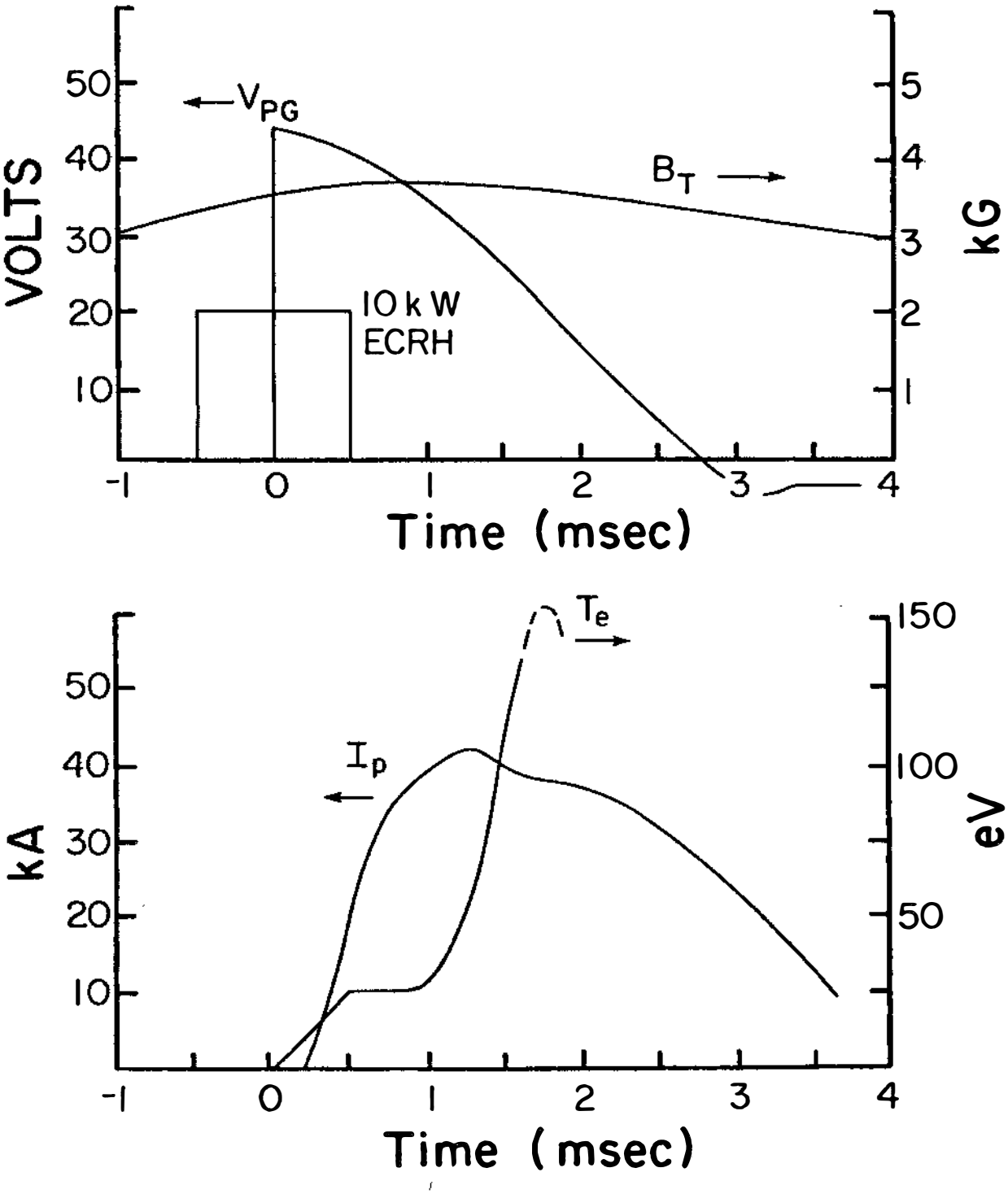
VOLTS
50
40
30
20
10
V_{PG}
B_T
10 k W
ECRH
5
4
3
2
1
kG
-1
0
1
2
3
4
Time (msec)
kA
50
40
30
20
10
I_p
T_e
150
100
50
eV
-1
0
1
2
3
4
Time (msec)

FIGURE 4

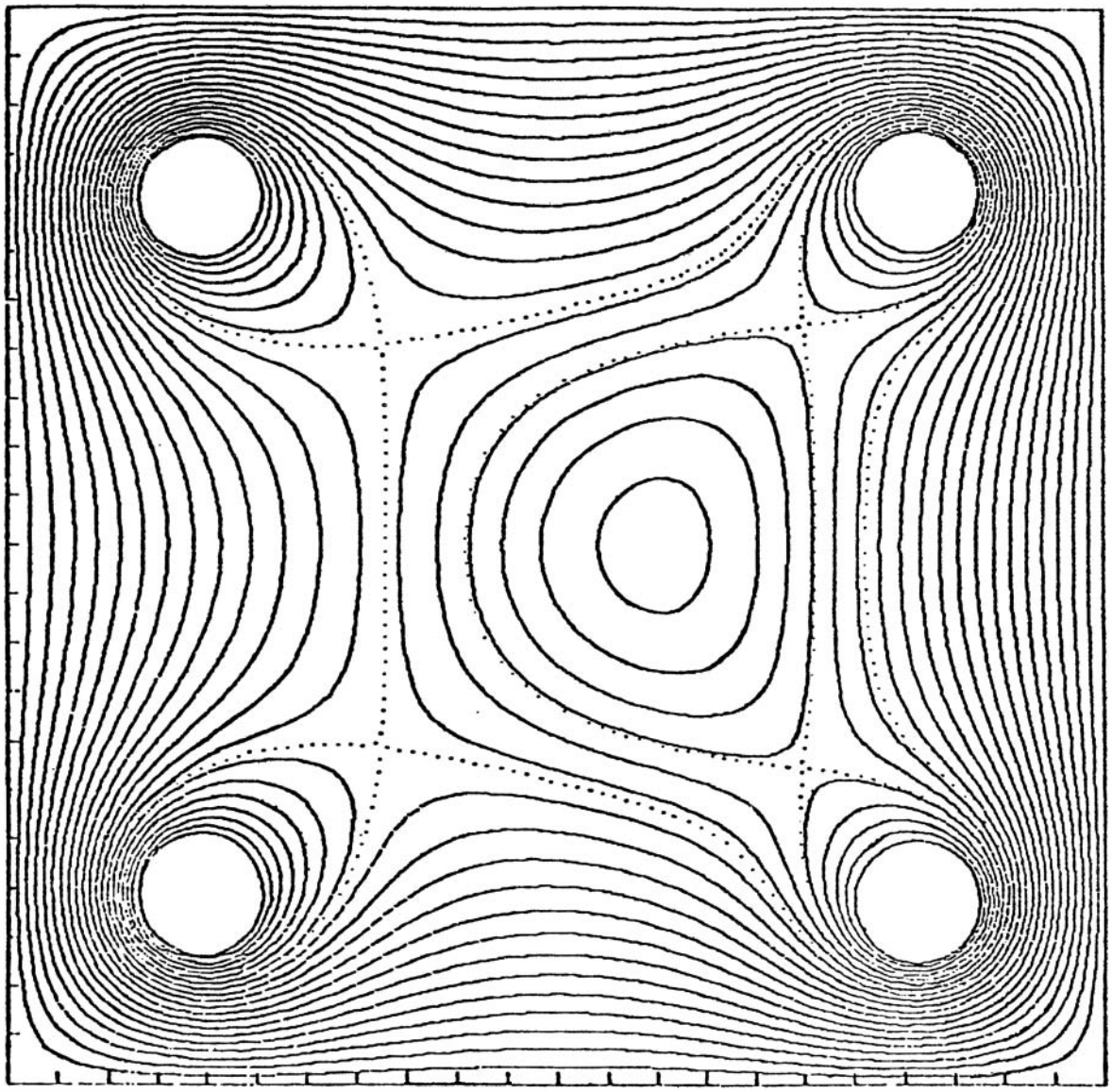

FIGURE 5

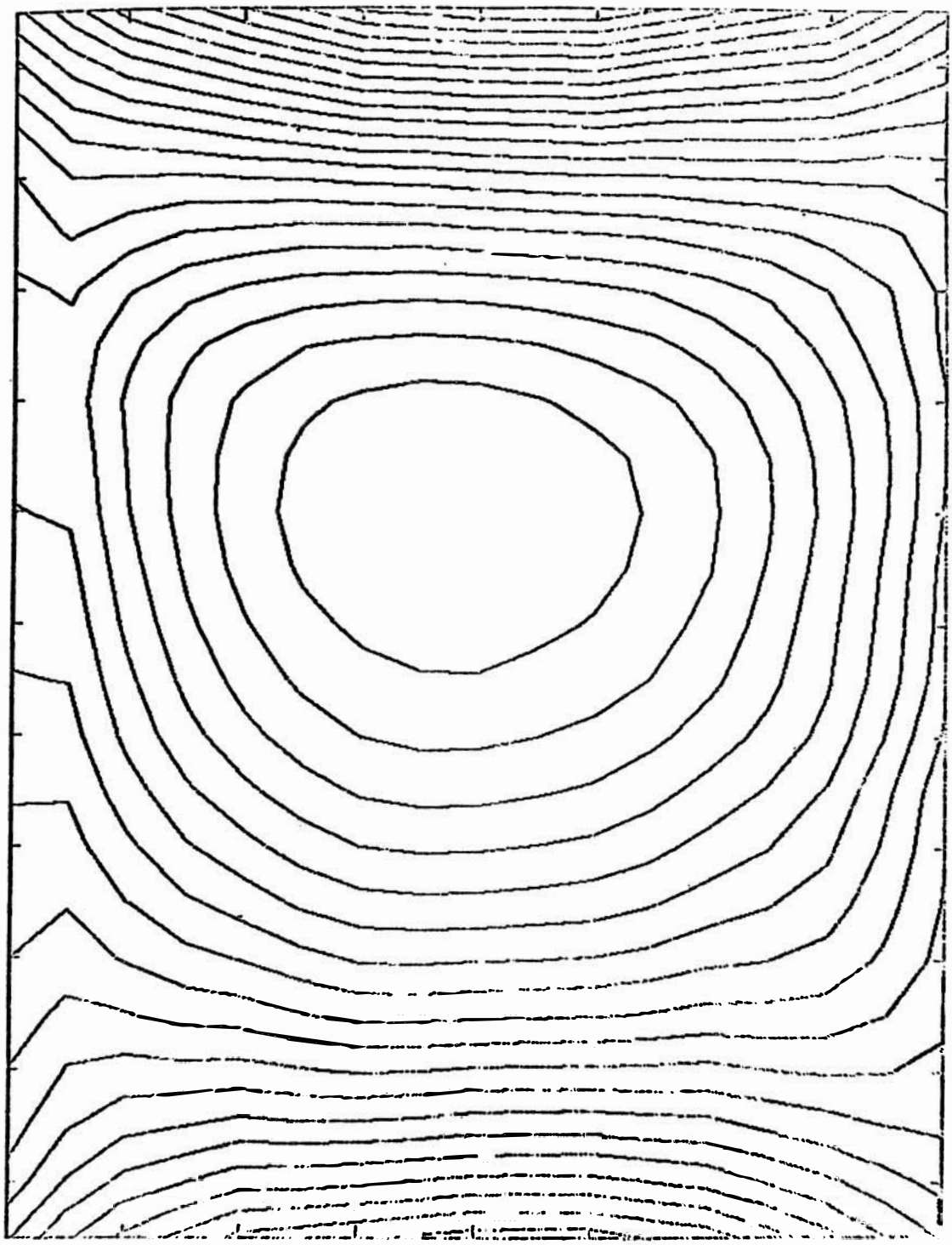

FIGURE 6

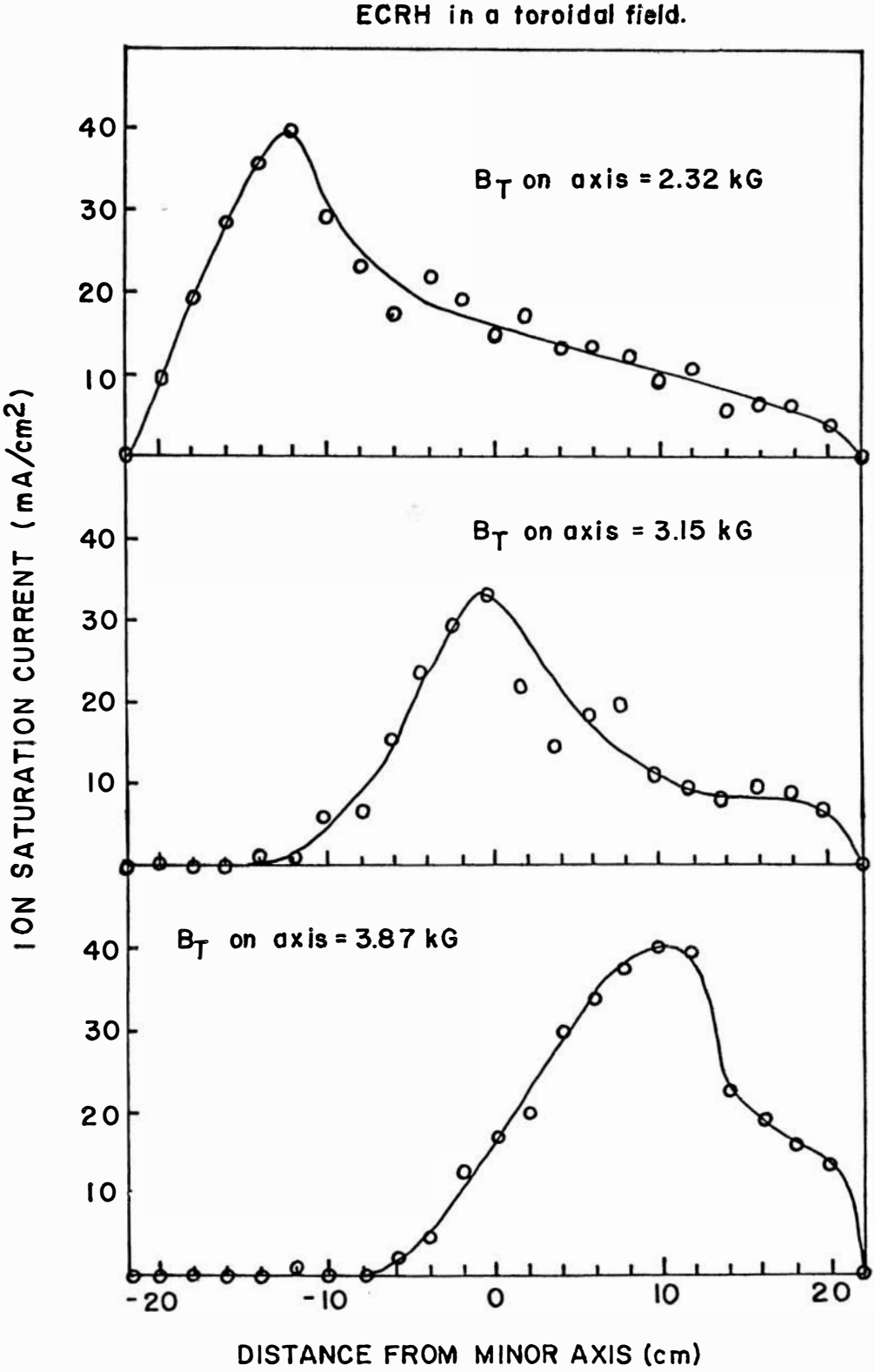
ECRH in a toroidal field.
B_T on axis = 2.32 kG
B_T on axis = 3.15 kG
B_T on axis = 3.87 kG
ION SATURATION CURRENT (mA/cm2)
DISTANCE FROM MINOR AXIS (cm)
40
30
20
10
-20
-10
0
10
20

FIGURE 7

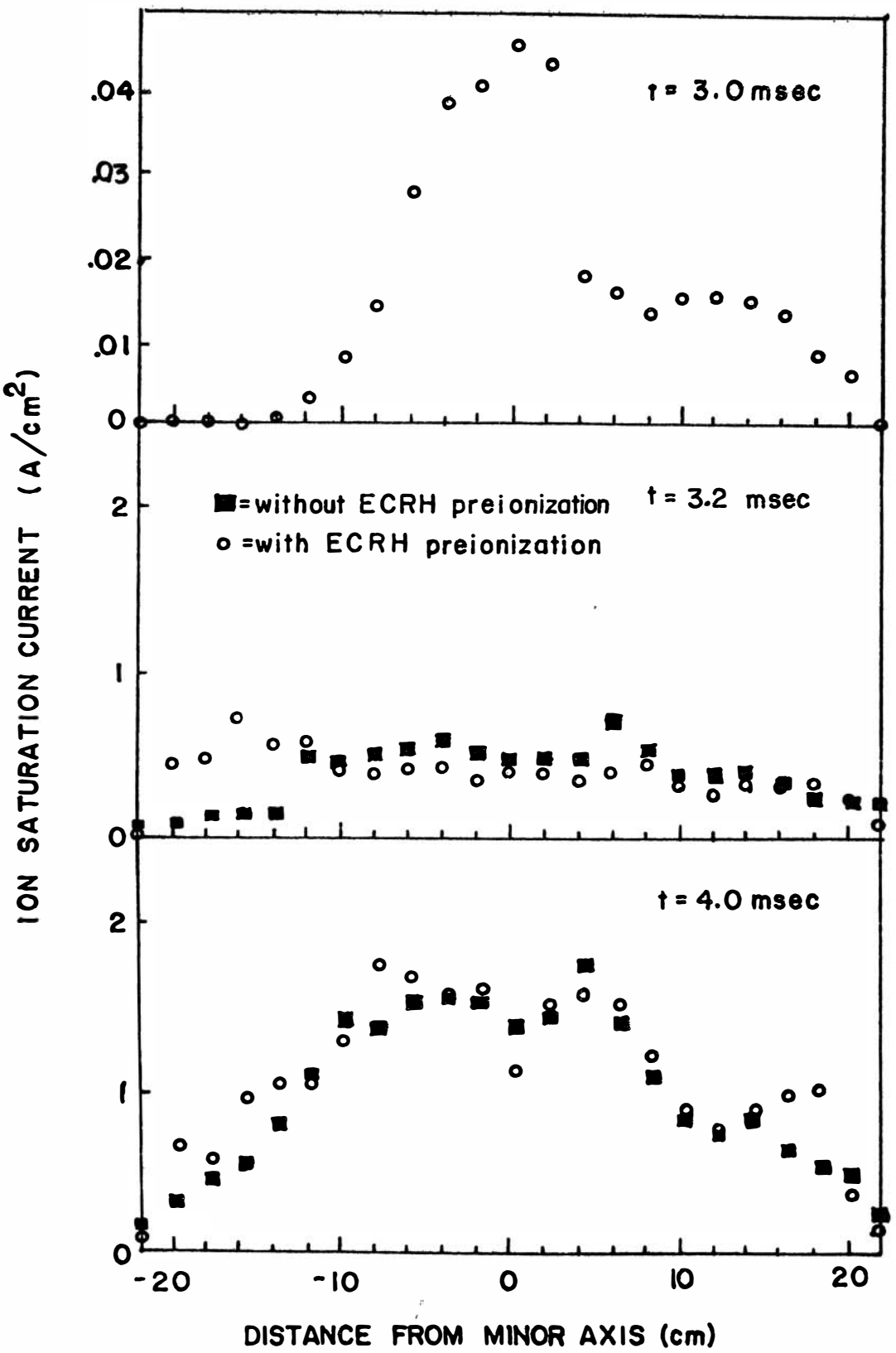
t = 3.0 msec
■ = without ECRH preionization
o = with ECRH preionization
t = 3.2 msec
t = 4.0 msec
ION SATURATION CURRENT (A/cm²)
DISTANCE FROM MINOR AXIS (cm)
.04
.03
.02
.01
0
2
1
0
2
1
0
-20
-10
0
10
20

FIGURE 8

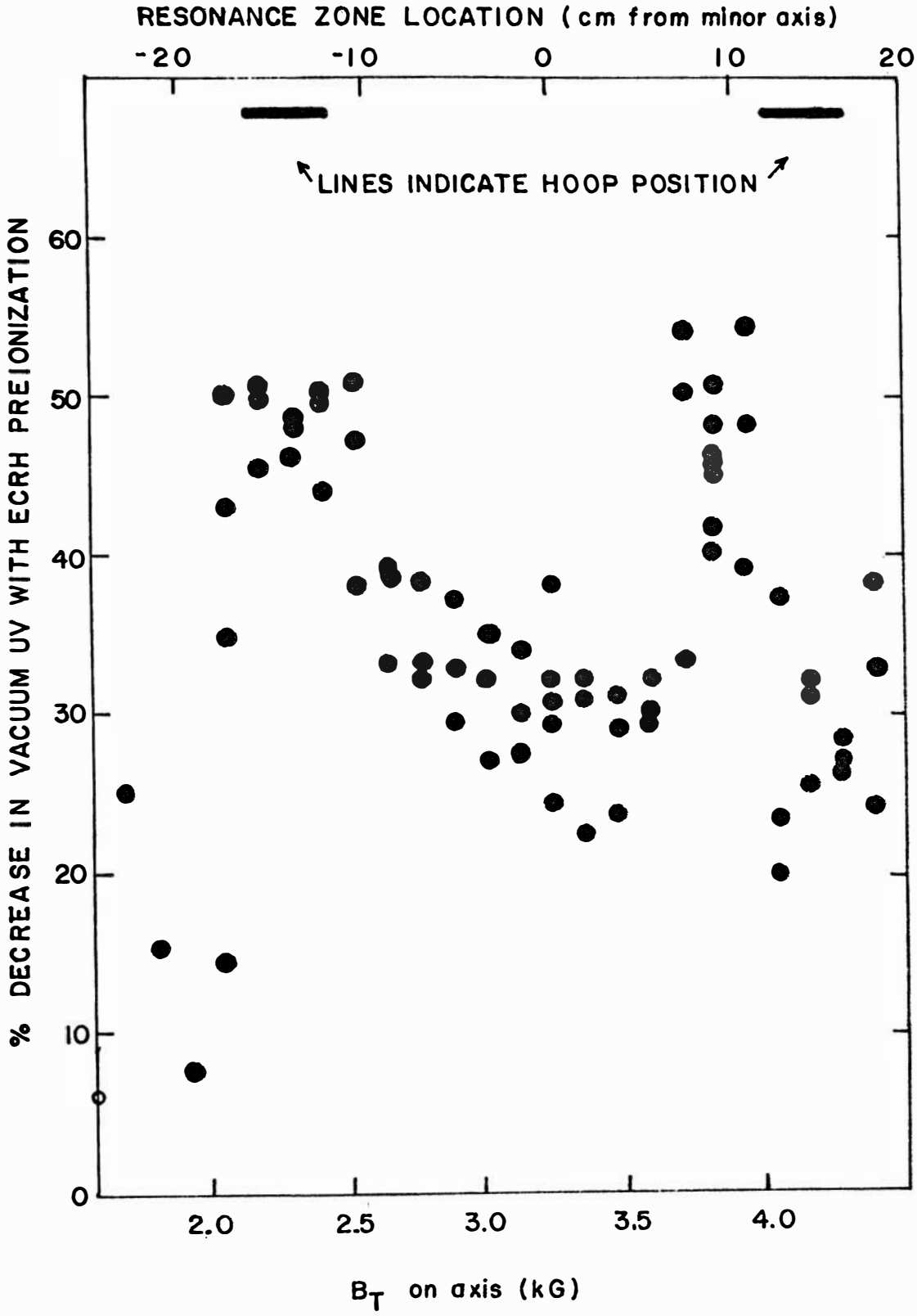
RESONANCE ZONE LOCATION (cm from minor axis)
-20
-10
0
10
20
LINES INDICATE HOOP POSITION
% DECREASE IN VACUUM UV WITH ECRH PREIONIZATION
60
50
40
30
20
10
0
2.0
2.5
3.0
3.5
4.0
B_T on axis (kG)

FIGURE 9

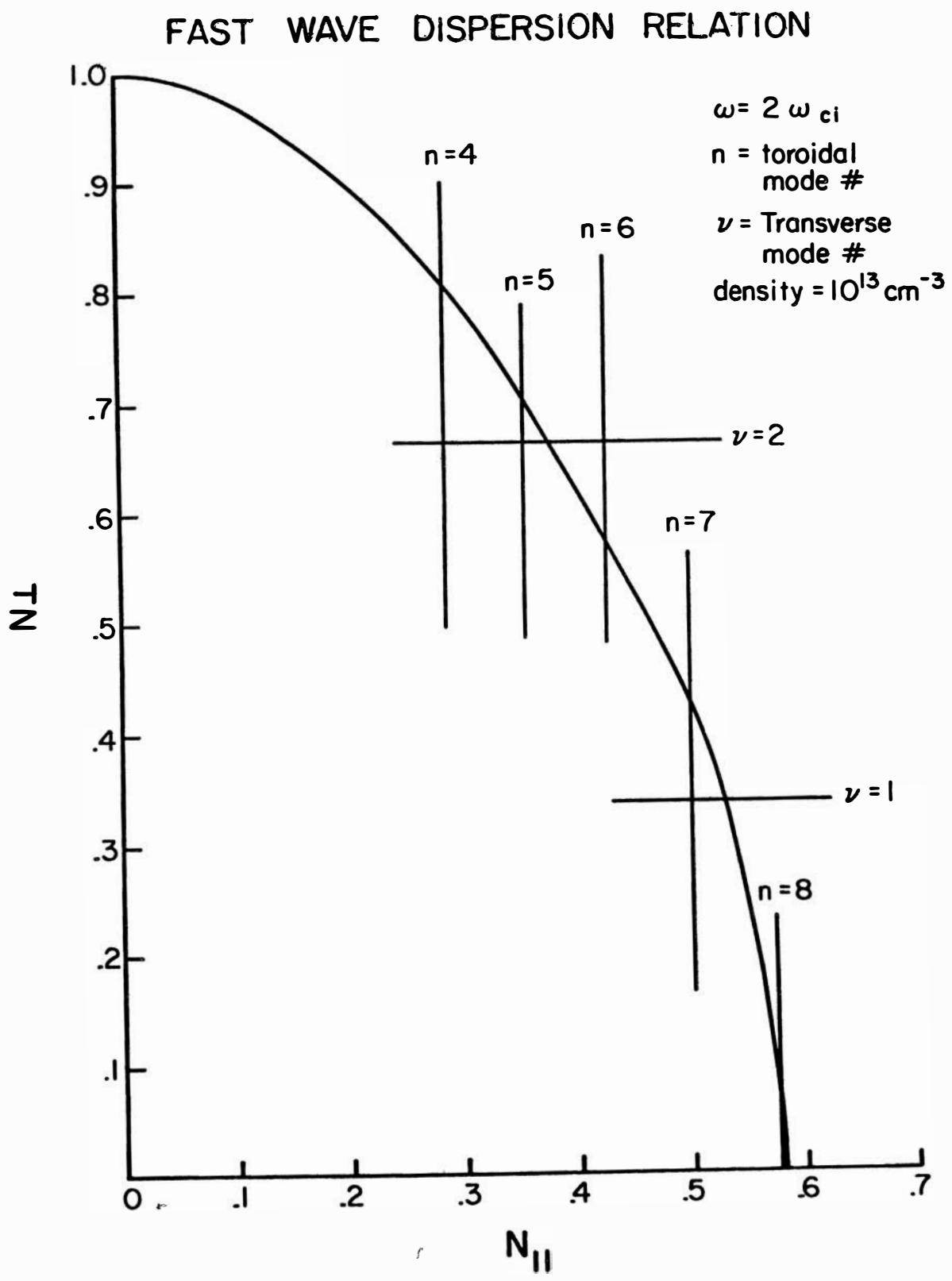
FAST WAVE DISPERSION RELATION
ω= 2 ω ci
n = toroidal mode #
ν = Transverse mode #
density = 10^13 cm^-3
n=4
n=5
n=6
n=7
n=8
ν=2
ν=1
1.0
.9
.8
.7
.6
.5
.4
.3
.2
.1
0
.1
.2
.3
.4
.5
.6
.7
TN
N||

FIGURE 10

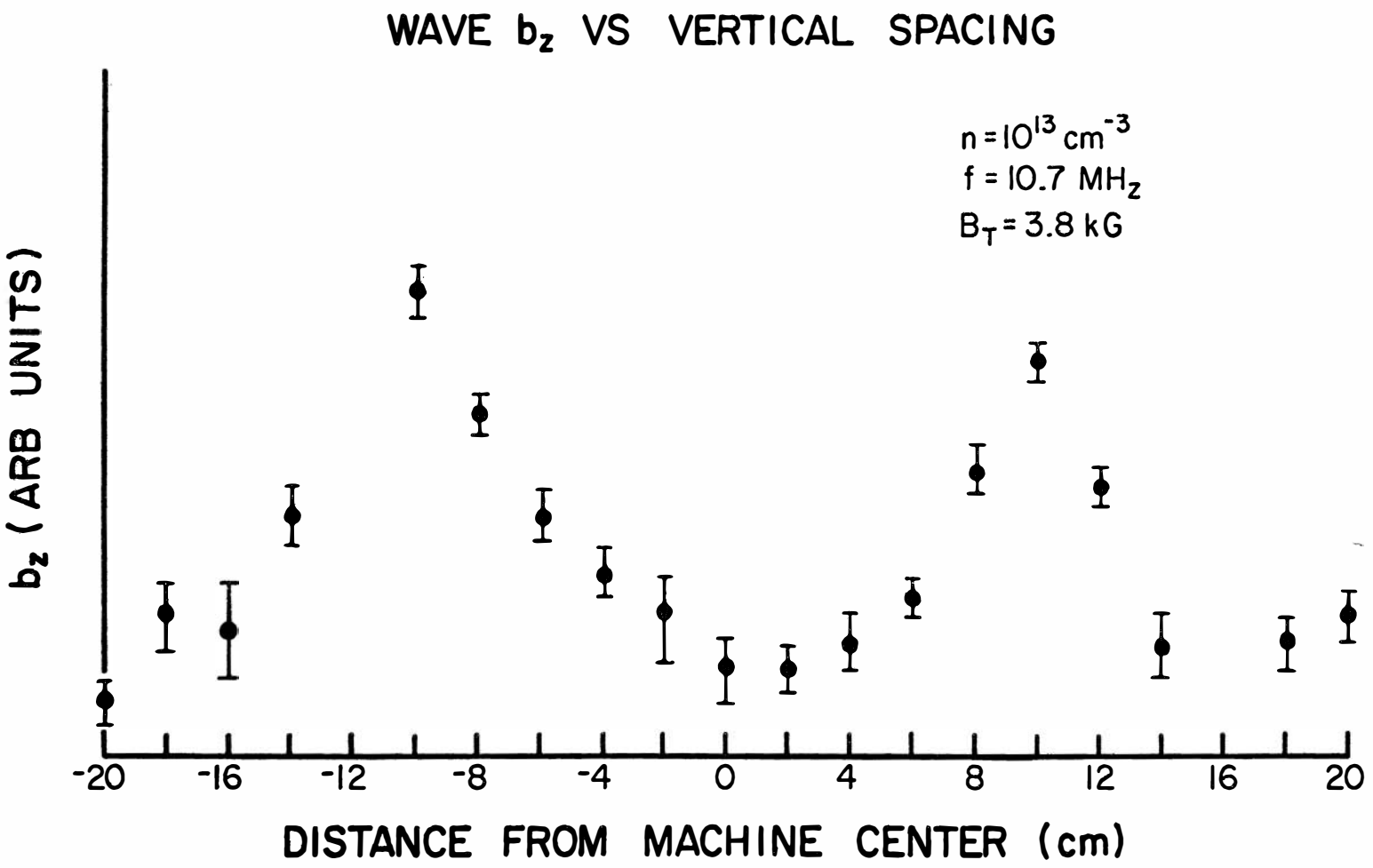
WAVE b_z VS VERTICAL SPACING
$n = 10^{13}\ cm^{-3}$
$f = 10.7\ MH_z$
$B_T = 3.8\ kG$
b_z (ARB UNITS)
-20
-16
-12
-8
-4
0
4
8
12
16
20
DISTANCE FROM MACHINE CENTER (cm)

FIGURE 11

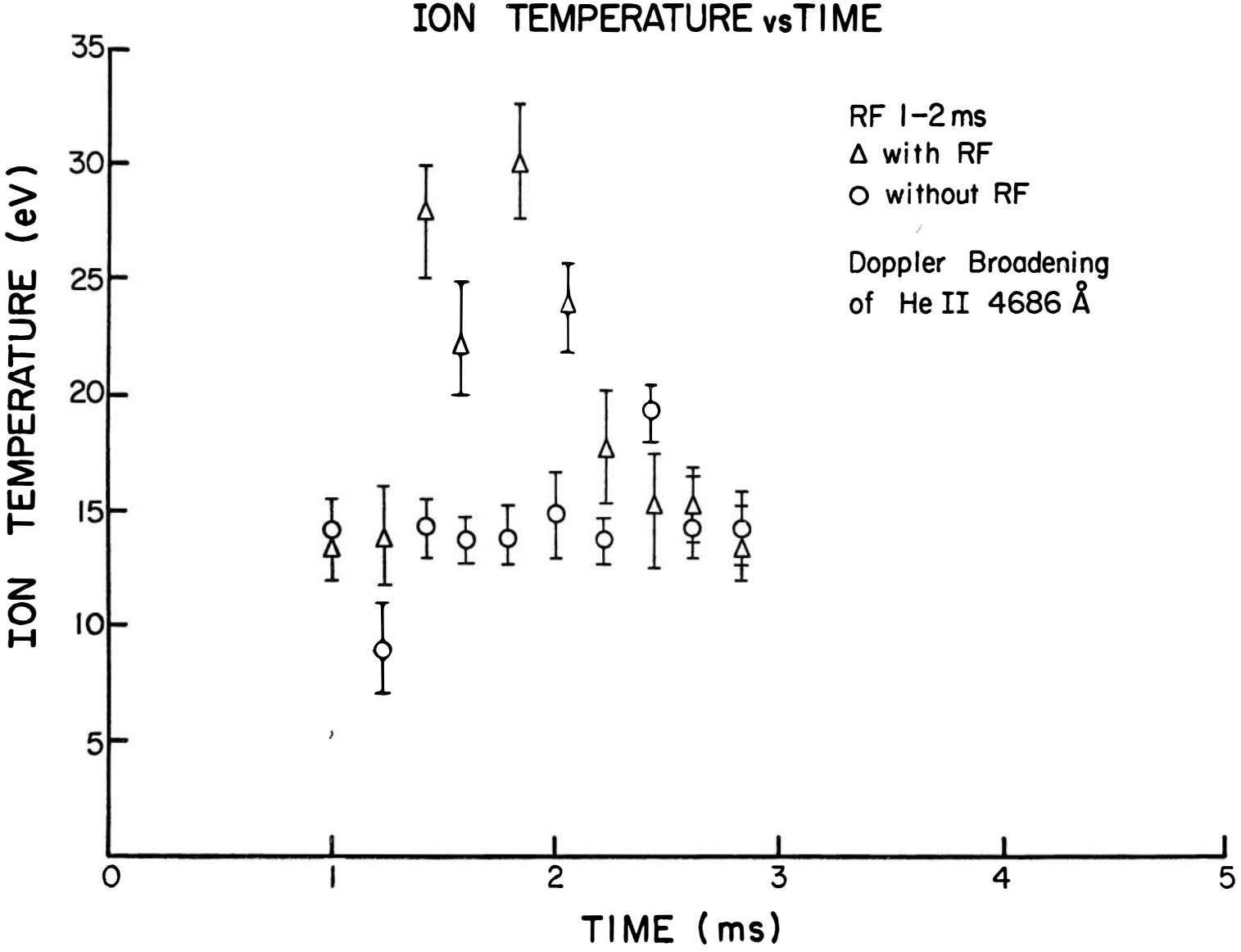
ION TEMPERATURE vsTIME
ION TEMPERATURE (eV)
35
30
25
20
15
10
5
0
1
2
3
4
5
TIME (ms)
RF 1-2 ms
Δ with RF
O without RF
Doppler Broadening
of He II 4686 Å

FIGURE 12

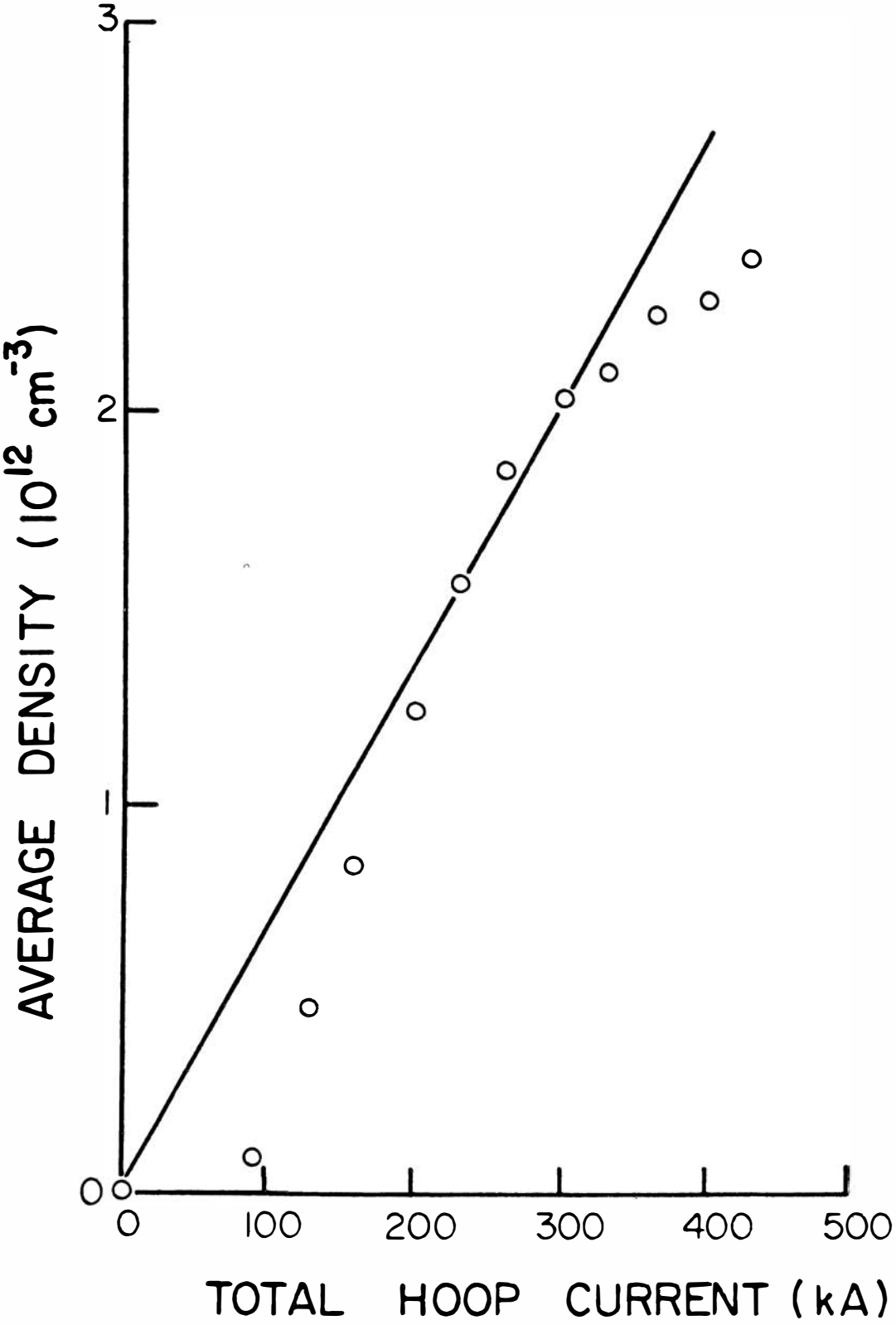
AVERAGE DENSITY (10^{12} cm^{-3})
3
2
1
0
0
100
200
300
400
500
TOTAL HOOP CURRENT (kA)

FIGURE 13

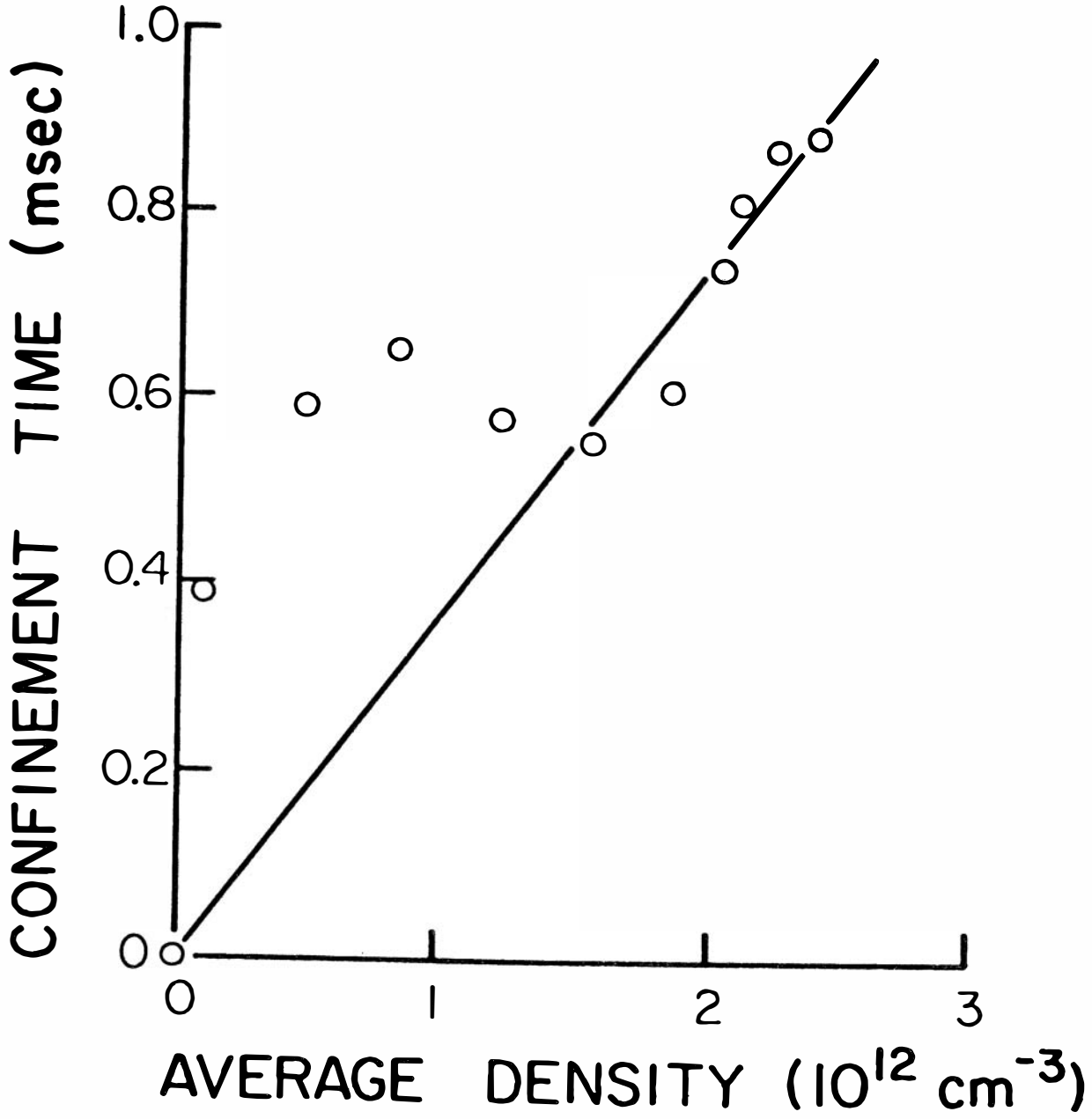
CONFINEMENT TIME (msec)
1.0
0.8
0.6
0.4
0.2
0
0
1
2
3
AVERAGE DENSITY (10^{12} cm^{-3})

FIGURE 14